Decementation, Softening, and Collapse: Changes in Small-Strain Shear Stiffness in k_0 Loading

Tae Sup Yun[1] and J. Carlos Santamarina[2]

Abstract: The small-strain stiffness of freshly remolded soils is controlled by the state of stress. Diagenesis and cementation can significantly stiffen soils. However, these effects are lost at relatively low strain levels. Previous experimental results have shown the detrimental and irrecoverable effects of unloading on cementation. This study explores the effect of k_0 loading on the small-strain stiffness of cemented specimens, with emphasis on the load-induced collapse and softening of cemented, loose soils. The evolution of collapse and decementation is monitored within an oedometric cell by means of small-strain shear wave propagation. Results highlight the interplay between stress-cementation history and initial void ratio. It is observed that the probability of collapse and decementation softening decreases with the increase in effective confinement at the time of cementation, the extent of cementation, and soil density. Volume collapse is preceded by stiffness loss. At high confinement, the stress-independent small-strain stiffness of initially cemented soils gradually converge to the stress-dependent stiffness that characterizes freshly remolded, uncemented soils.

DOI: 10.1061/(ASCE)1090-0241(2005)131:3(350)

CE Database subject headings: Aging; Brittleness; Cementation; Shear waves; Stiffness.

Introduction

Most soils experience some level of diagenesis and cementation. These processes increase the contact area between particles and bond neighboring particles together. Light cementation is often sufficient to significantly increase the small-strain stiffness of soils, their dilative tendency, and the resistance to liquefaction. As the degree of cementation increases, the drained strength is impacted as well.

Therefore, cementation can have a profound effect on analysis and design. On the one hand, more economical designs may be achieved when cementation is recognized; for example, a lower cost shallow foundation system may be sufficient to satisfy deformation requirements, or expensive ground improvement may not be needed to prevent liquefaction (high small-strain stiffness of cemented soils hinders the early buildup of pore-water pressure). On the other hand, the misinterpretation of cementation effects can lead to unsafe design; for example, high seismic velocity does not necessarily imply a strong foundation layer, loose lightly cemented soils often exhibit collapse, and progressive failure may accompany shear. These examples show the need for proper site characterization, improved laboratory test procedures that take into consideration sampling effects, and adequate engineering design criteria and models.

[1]Graduate Student, Dept. of Civil and Environmental Engineering, Georgia Institute of Technology, Atlanta, GA 30332.

[2]Professor, Dept. of Civil and Environmental Engineering, Georgia Institute of Technology, Atlanta, GA 30332.

Note. Discussion open until August 1, 2005. Separate discussions must be submitted for individual papers. To extend the closing date by one month, a written request must be filed with the ASCE Managing Editor. The manuscript for this paper was submitted for review and possible publication on February 14, 2003; approved on July 14, 2004. This paper is part of the ***Journal of Geotechnical and Geoenvironmental Engineering***, Vol. 131, No. 3, March 1, 2005. ©ASCE, ISSN 1090-0241/2005/3-350–358/$25.00.

Particle debonding and skeletal softening are readily observed under triaxial loading conditions (e.g., Airey and Fahey 1991). Debonding and softening can also take place during unloading, even under isotropic conditions: soils cemented under confinement expand during unloading and the cement at interparticle contacts fails in tension [numerical observations in Zang and Wong (1995); experimental observations in Fernandez and Santamarina (2001)]; this is an inherent mechanism in sampling (data in Tatsuoka and Shibuya 1991).

Available cemented soil response data under k_0 loading (e.g., Shibuya et al. 2001; Leroueil and Hight 2003) do not permit analyzing the development of debonding, softening, and collapse. The purpose of this study is to explore the evolution of small-strain stiffness in lightly cemented loose and dense soil specimens subjected to k_0 loading. Special emphasis is placed on identifying the association between stiffness loss and structural collapse upon loading. This study starts with a brief review of prior studies on cemented soils. Then the experimental methodology designed to study k_0 loading effects is presented followed by results and discussion.

Brief Review of Prior Studies

Previous studies show that the effect of cementation on soil behavior depends on the amount and type of cementing agent, the grain size distribution of the soil (the higher the specific surface, the thinner the layer of cement around grains), density (interparticle coordination increases with density), and the degree of confinement at the time of cementation, i.e., the stress-cementation history (Clough et al. 1981; Winkler 1983; Acar and El-Tahir 1986; Feda 1995; Baig et al. 1997; Jarrad et al. 2000).

Cementing agents can deposit evenly around particles. However, cementation has a maximum influence on the granular skeleton when cementing processes develop at contacts. This is the case when cementation is triggered by drying (a retracting capillary meniscus causes fines migration and aggregation and salt

precipitation at the contact), or when it is associated with phenomena such as contact yield, sintering, and solution precipitation (Bernabe et al. 1992). When a cementing agent precipitates around interparticle contacts, the load-induced stress distribution at the composite contact depends on the stiffness of the minerals that make the grains (E_{min}) and the cementing material (E_{cem}). Disregarding geometric effects: when $E_{min}/E_{cem}=1$, the stress changes at the contact follows Hertzian behavior; when $E_{min}/E_{cem} \gg 1$, the mineral contact picks up the new load; and when $E_{min}/E_{cem} \ll 1$, stress concentration develops within the cementing material (Dvorkin and Yin 1995; Zang and Wong 1995; Sienkiewicz et al. 1996). In all cases, the cement is load bearing; hence, it reduces the stress concentration within particles, and increases the crushing strength of the soil (Yin and Dvorkin 1994; Dvorkin and Yin 1995).

Two stress regimes can be identified. Under low confinement, the behavior of the cemented soil is cementation controlled, and the soil exhibits the following characteristics:

1. The drained load deformation behavior is brittle (Lade and Overton 1989; Airey and Fahey 1991).
2. Cementation controls the drained peak strength, and the shear strength intercept increase with cement content (Dupas and Pecker 1979; Clough et al. 1981; Acar and El-Tahir 1986; Dass et al. 1994).
3. Postpeak, strain softening is often accompanied by strain localization (Schanz 1998).
4. Interparticle bonds begin breaking prior to the peak strength of the soil (Feda 1995). Debonding forms an interlocked blocky structure and the soil is more prone to dilate (Wissa and Ladd 1965; Saxena and Lastrico 1978; Saxena et al. 1988; Lade and Overton 1989).
5. Stiffness is cementation controlled and quasistress independent as in a linear solid (Baig et al. 1997).

Under high confinement, the soil response is stress controlled:

1. The small-strain stiffness increases as confinement increases (even in the absence of debonding), approaching the power relation that characterizes freshly remolded granular materials (e.g., Hardin and Richart 1963)

$$G_{max} = \Lambda \left(\frac{\sigma'_m}{1\ \text{kPa}} \right)^{\zeta} \tag{1}$$

   where σ'_m = mean effective stress on the shear plane; Λ = stiffness at $\sigma'_m = 1$ kPa; and ζ = exponent (both Λ and ζ are experimentally determined).
2. The large-strain load–deformation behavior changes towards a ductile, strain hardening response.
3. The effective peak angle of shear strength ϕ'_{peak} is not significantly changed by the degree of initial cementation (Wissa and Ladd 1965; Acar and El-Tahir 1986; Saxena et al. 1988; Reddy and Saxena 1993).

In both confining stress regimes, the shear resistance gradually changes from cohesive to frictional as the imposed strain progresses and debonding takes place. Acoustic emission counts associated with particle debonding decisively increase beyond 75–85% of the peak load (Landis and Shah 1995). Therefore, the large-strain strength is characterized by $c=0$ and residual friction angle ϕ_{res}, and it is independent of the degree of initial cementation in both low and high confinement regimes (Clough et al. 1981). The transition stress between these two regimes increases as the cement content increases (Saxena et al. 1988; Dass et al. 1994; Baig et al. 1997).

The small strain stiffness of particulate materials is determined by the deformability of interparticle contacts due to stress concentration. From Hertzian contact theory, the small-strain stiffness of the granular skeleton (E_{skel}) is (e.g., Richart et al. 1970)

$$E_{skel} = \frac{r_c}{R} \cdot \frac{G_g}{(1-\nu_g)} \tag{2}$$

where r_c = radius of the contact area (a measure of contact flatness); R = particle radius; and G_g and ν_g = shear modulus and Poisson's ratio of the mineral that makes the particles. Eq. (2) highlights the importance of contact flatness (captured in r_c), regardless of the mechanism that causes it. In fact, applied confinement, cementation, or even the viscous creep of the grain renders higher skeletal stiffness. Furthermore, Eq. (2) explains the high sensitivity of small-strain soil stiffness E_{skel} to cementation, and the particularly beneficial effect of cement localization at interparticle contacts, thus effectively increasing r_c. [See Fernandez and Santamarina (2001) for a detailed application of Eq. (2) to cemented soils taking into consideration the cementation–stress history.] In this study, the small-strain shear stiffness G_{max} is inferred from shear wave velocity V_s measurements

$$G_{max} = \rho V_s^2 \tag{3}$$

where ρ = mass density of the medium.

Table 1. Specimen and Test Characteristics

Test Number	e_o	σ'_{sit}(kPa) during cementation	σ'_{max} (kPa)	Cement (%)	Number of loading/ unloading steps
1	0.782	-	1,062.5	0	10/9
2	1.139	18.7	1,071.1	2	8/8
3	1.154	18.7	1,071.1	4	8/8
4	0.953	122.8	1,053.8	2	5/8
5	0.575	-	1,062.5	0	10/9
6	0.695	18.7	1,071.1	2	8/8
7	0.714	18.7	1,071.1	4	8/8
8	0.636	122.8	1,053.8	2	5/8

Experimental Design

Artificially cemented sands are used for this study, and subjected to k_0 loading in a zero-lateral strain oedometric cell. Material, devices, and procedures are described next.

Sample Preparation

Uniform, fine, angular sand is used to evaluate the behavior of cemented soils (Nevada sand, $e_{min}=0.533$, $e_{max}=0.888$, mean grain size $D_{50}=0.14-0.17$ mm, uniformity coefficient $C_u=1.67$). The cementing agent is Portland cement Type I (specific gravity $G_s=3.15$). Eight samples are prepared with different initial void ratio, cement content, and initial vertical stress at the time of cementation herein called the vertical sitting pressure σ'_{sit}. The initial void ratio, the vertical sitting pressure, the maximum load, and the number of loading and unloading steps for each test are summarized in Table 1. All tests are successfully duplicated to verify repeatability.

The sand is oven dried for 24 h before testing. Uncemented soil specimens are prepared in the oedometric cell by funneling

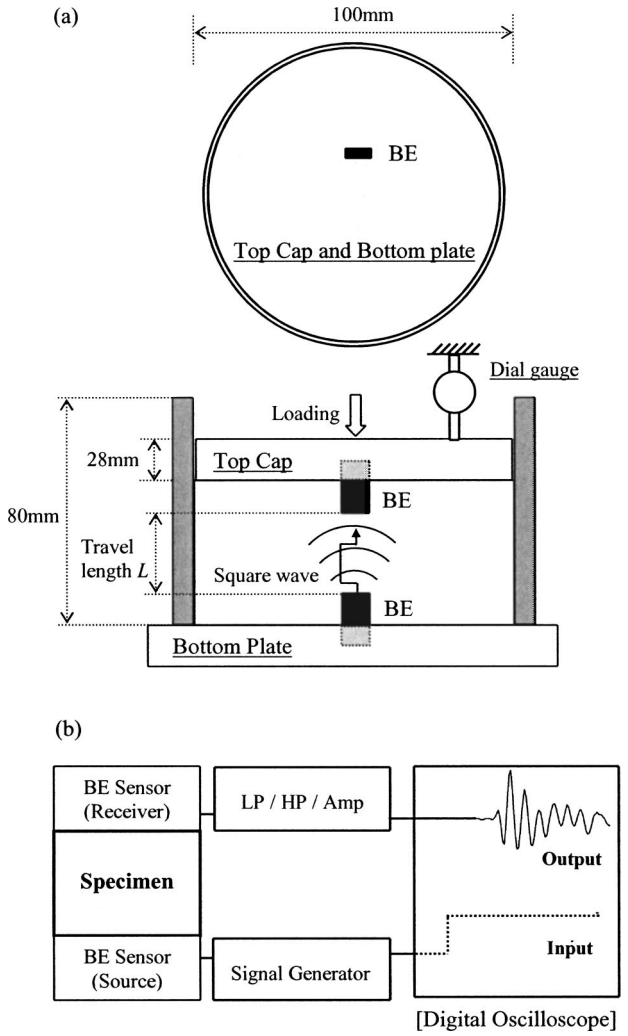

Fig. 1. Oedometer cell: (a) top cap and bottom plate of oedometer cell where bender elements are housed and (b) peripheral electronics

and tamping methods to attain either loose or dense conditions. When tamping is used, the same weight of soil is added to form each layer.

Artificially cemented soils are prepared by thoroughly mixing the cement and the sand; afterwards, a predetermined amount of water is added to the mixture. The wet mixture is homogenized for 5 min and gradually scooped into the cell or tamped to produce loose and dense specimens. These specimens have higher void ratios than the corresponding uncemented, dry specimens due to interparticle capillary forces that prevent compaction. Capillary stabilization is most pronounced in the loose specimens, which are placed without tamping (Rao et al. 1995).

Once the cell is filled, the upper plate is placed on top of the specimen and the initial void ratio is determined.

Test Devices

The bottom plate and the top cap of the oedometric cell house the bender element pair. Each bender element is electrically shielded and grounded to prevent electrical cross talk. Cell details are shown in Fig. 1 [design documented in Fam and Santamarina (1995) and see Shirley and Hampton (1978); Dyvik and Madshus (1985); Thomann and Hryciw (1990) and Kuwano and Jardine (2002) for a discussion on bender element configuration and performance].

A signal generator (Krohn-Hite 1400A) delivers a 20 Hz square wave. The signal captured with the receiver bender element is fed through a filter–amplifier (Krohn-Hite 3364, low-pass filter at $f=50$ kHz and high-pass filter at $f=100$ Hz) into the digital storage oscilloscope (Rapid Systems R1016), where signals are digitized at 200 kHz sampling frequency. The stacking of 256 signals permits reducing the non-coherent noise.

Test Procedure

The applied load is incrementally doubled at each loading stage reaching a maximum vertical effective stress of $\sigma'_{max} \cong 1$ MPa. Each loading stage lasts 10–15 min. Shear wave velocity is measured at the end of this period before increasing the load. The same procedure is implemented during unloading.

The vertical sitting pressure σ'_{sit} is reached before cement hardens (within 40 min after mixing), and it is maintained constant during the 24 h hardening period; either $\sigma'_{sit}=18.7$ or $\sigma'_{sit}=122.8$ kPa is used (Table 1).

The time at "first arrival" t_{first} is picked from the stored time series, taking into consideration near field effects (Sánchez-Salinero et al. 1986). The travel length L is taken as the tip-to-tip distance between bender elements (Fig. 1). Finally, the shear wave velocity is computed as $V_s=L/t_{first}$.

After testing, specimens are observed with an optical microscope (Qimaging micropublisher 32-0028A-211) to identify the effects of loading or load-induced decementation.

Experimental Results

Time series are presented for three characteristic cases. Fig. 2 shows the variation in travel time during loading and unloading in uncemented specimens. In contrast, Fig. 3 shows almost constant signatures for all load levels in the 4% cement specimen. Finally, Fig. 4 presents the time series for the 2% loose specimen cemented at low vertical sitting pressure. The sudden increase in travel time during loading in this specimen denotes the breakage of cementing bonds; there is also a marked increase in travel time during unloading, resembling the trend for the uncemented specimen in Fig. 2. To facilitate the interpretation of results, velocity–stress and volume change trends are presented next.

Velocity–Stress Behavior

Uncemented Soils

The shear wave velocity of uncemented soils increases as the vertical effective stress increases. Velocity–stress data during loading and unloading are shown in Fig. 5(a) for loose and dense sands. Combining Eqs. (1) and (3), the velocity–stress relation for uncemented soils becomes $V_s=\alpha\cdot\sigma'^{\beta}_m$, where σ'_m=mean stress in the polarization plane that is the vertical applied stress times $(1+k_0)/2$. Data points are least squared fitted to determine α and β parameters: for loose sands $\alpha=48$ m/s and $\beta=0.248$; for dense sands, the corresponding parameters are $\alpha=68$ m/s and $\beta=0.192$. These values agree with published results for similar sands (compilation in Santamarina et al. 2001). The unloading trends plot above the loading trends because horizontal stresses are locked in the sand.

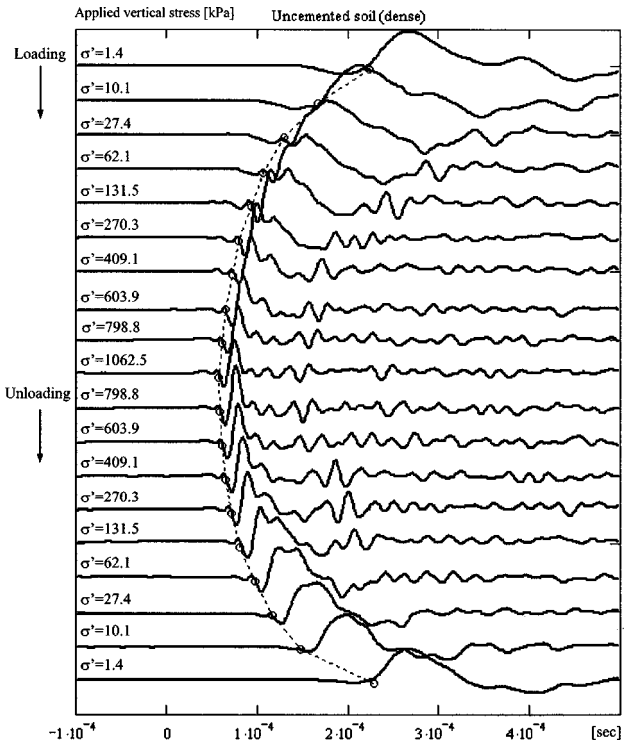

Fig. 2. Evolution of shear wave time series during loading and unloading dense uncemented soil specimen (initial void ratio $e_o=0.782$)

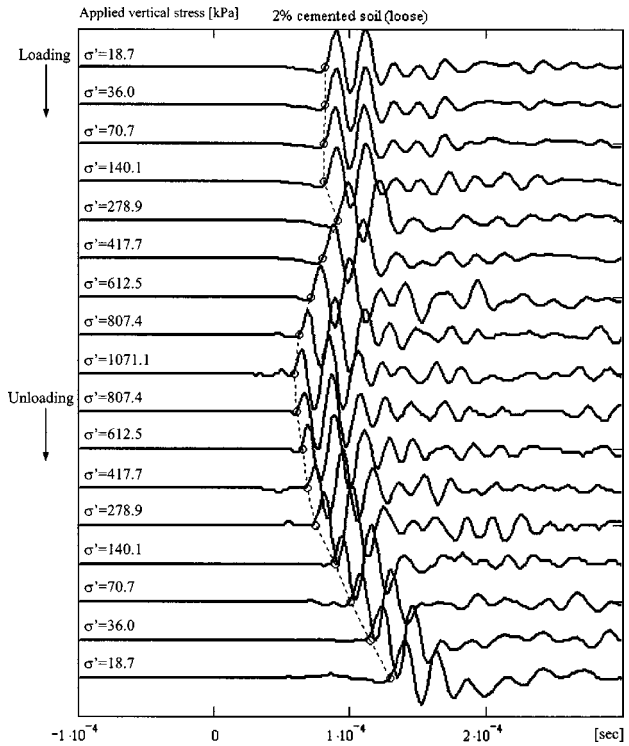

Fig. 4. Evolution of shear wave time series during loading and unloading loose, cemented soil specimen (initial void ratio $e_o=1.139$, cement content: 2%, vertical sitting pressure during hardening $\sigma'_{sit}=18.7$ kPa)

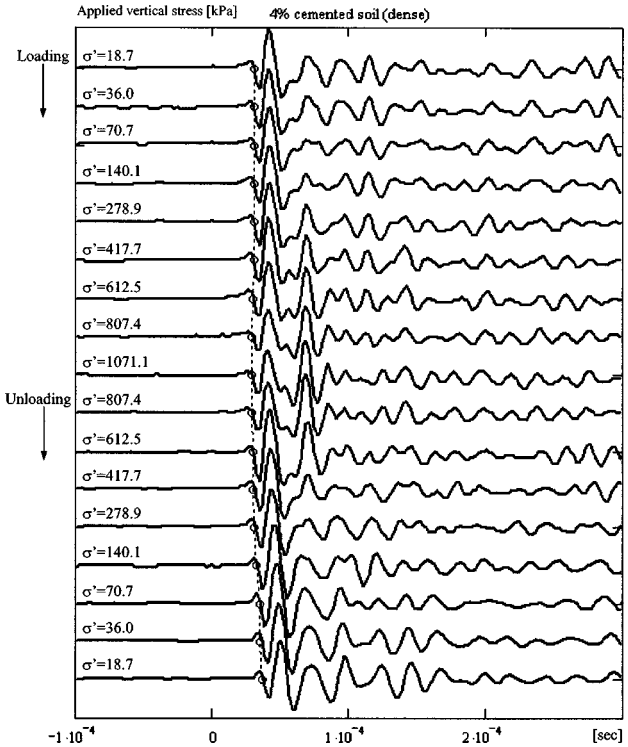

Fig. 3. Evolution of shear wave time series during loading and unloading dense, cemented soil specimen (initial void ratio $e_o=0.714$, cement content: 4%, vertical sitting pressure during hardening $\sigma'_{sit}=18.7$ kPa)

Loose Cemented Soils

The 2% cemented loose sand under an initial vertical sitting pressure of $\sigma'_{sit}=18.7$ kPa shows a distinctly different trend from the uncemented specimen [Fig. 5(b)]. At the beginning of loading, until a vertical effective stress $\sigma'_v \cong 140$ kPa, the shear wave velocity increases very slightly, and then additional load causes the collapse of the specimen and a significant decrease in stiffness. During further loading, the velocity never drops below that of the uncemented soil and increases with stress. The loading and unloading trends cross; this is not observed in uncemented soils.

The 2% cemented loose soil specimen formed under high initial vertical pressure, $\sigma'_{sit}=122.8$ kPa, permits assessing the importance of sitting pressure relative to cementation (the sitting pressure is six times higher than in the previous specimen). During early confinement prior to cementation, in Fig. 5(c), the velocity increases with stress as in uncemented soils (albeit with higher values due to increased interparticle capillary forces). Cement hardening after 24 h renders a velocity higher than for the 2% cement specimen cured at low confinement [Fig. 5(c)]. Loading after hardening does not cause a velocity drop. However, the unloading trend runs below the loading trend in the range $\sigma'_{sit} < \sigma'_v < \sigma'_{max}$ suggesting loss of cementation.

The increase in velocity during hardening for the 4% cemented loose specimen is much higher than for either of the 2% cemented loose specimens [low and high sitting pressure Fig. 5(d)]. First, the velocity remains fairly constant during loading, and then falls during collapse decementation and increases again upon further loading. The 4% cement specimen collapses at around 450–500 kPa, which is three times higher than the collapse load

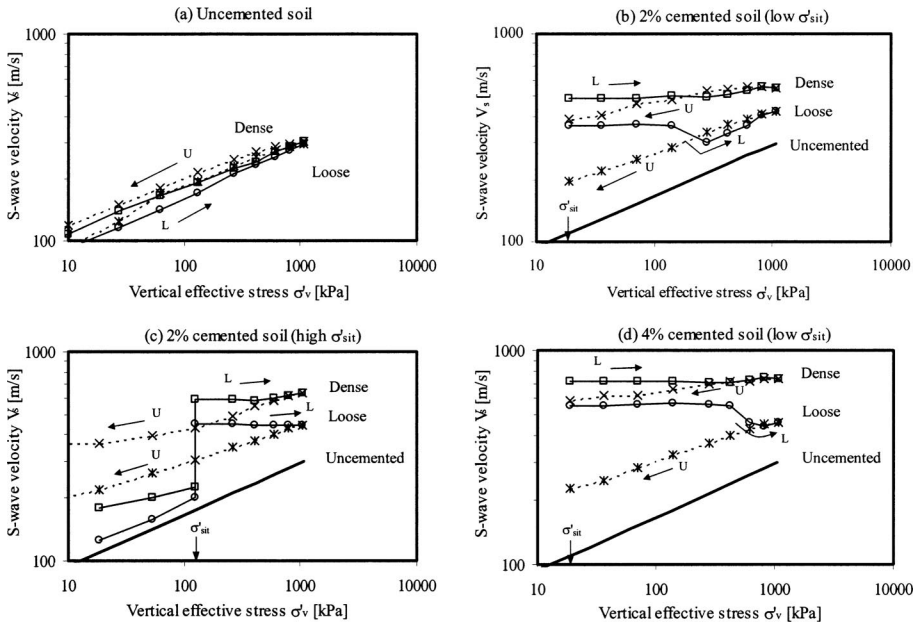

Fig. 5. Shear wave velocity versus vertical effective stress—summary. Note: log–log plot highlights global trends but diminishes effect of collapse on stiffness: (*L*) solid line loading, (*U*) dotted line unloading (initial vertical sitting pressures during hardening σ'_{sit}=18.7 kPa and σ'_{sit}=122.8 kPa).

for the 2% cement soil. The shear wave velocity during unloading reaches much lower values than those observed during loading at similar confinement.

Dense Cemented Soils

The specimens prepared with 2 and 4% cement and dense packing show similar trends as the loose cemented specimens during cementation. Decementation collapse is either absent in dense specimens or less defined than in loose specimens. At any given stress, the velocity V_s is higher in dense specimens than in the corresponding loose specimens. During unloading, the shear wave velocity remains lower than during loading, indicating that some decementation has taken place.

Volume Change—Threshold Vertical Strain

The $e-\sigma'_v$ response is a fingerprint of the evolution of decementation and collapse (Fig. 6) (see also Feda 1982; 1994). For reference, data for uncemented loose and dense specimens are presented in Fig. 6(a). During early stages of loading when the interparticle cementation contributes to load bearing, the cemented soil behaves elastically, albeit not necessarily linearly. Once the vertical applied stress reaches the decementation–collapse load (or yield vertical stress σ'_y) of loose specimens, a significant reduction in void ratio is observed for both the 2 and 4% cemented loose soils [Figs. 6(b and d)]. The collapse load increases with the amount of cement from σ'_y=140 kPa for the specimen with 2% cement to σ'_y=450–500 kPa for the one with 4% cement. The threshold vertical strain on the verge of collapse decementation ε_{th} is estimated from the initial void ratio (e_o) and the change in void ratio to the moment when collapse starts $\varepsilon_{th}=(e_o-e)/(1+e_o)$. Almost identical values are obtained from duplicate tests: ε_{th}=0.002 for the 2% cement specimens, and ε_{th}=0.003–0.004 for the 4% cement specimens. Therefore, these data suggest that the collapse stress and the associated threshold vertical strain for collapse decementation increases with cement content (Note that this is not the strain at peak strength, see for example Clough et al. 1981; Lade and Overton 1989).

Dense specimens do not exhibit collapse in e-log σ'_v [Figs. 6(b, c, and d)]. These specimens have higher interparticle coordination number, experience small strain upon loading, and can better preserve interparticle bonds to high stress levels.

Optical Observations

Specimens are removed from the oedometric cell after final unloading. The loose cemented soil specimens are broken with a blocky structure suggesting partial decementation. The dense cemented soil specimens remain as a monolith stack to the cell, and decementation is not visually apparent. Particle crushing is not observed.

Additional Observations

Load-induced decementation and collapse are simultaneously explored in the V_s-e plots for all specimens shown in Fig. 7. The trajectory is concave upwards; that is, decementation softening takes place prior to collapse.

The amount of cementation is the most important factor on shear wave velocity, while density and pressure exert a lesser influence. For example, the dense 2% cement specimen cured under 122.8 kPa (high) vertical sitting pressure reaches a lower shear wave velocity than the dense 4% cement specimen cured under 18.7 kPa (low) vertical sitting pressure [Fig. 5(c and d)]. In fact, the cemented specimens exhibit higher shear wave velocity than the uncemented specimens at the same stress level, even after collapse and decementation.

The stiffening effect of capillary interparticle forces is clearly seen in soil–cement mixtures prior to cement hardening: menisci that form at grain-to-grain contacts add a compressive interparticle force and the shear wave velocity increases. Experimental

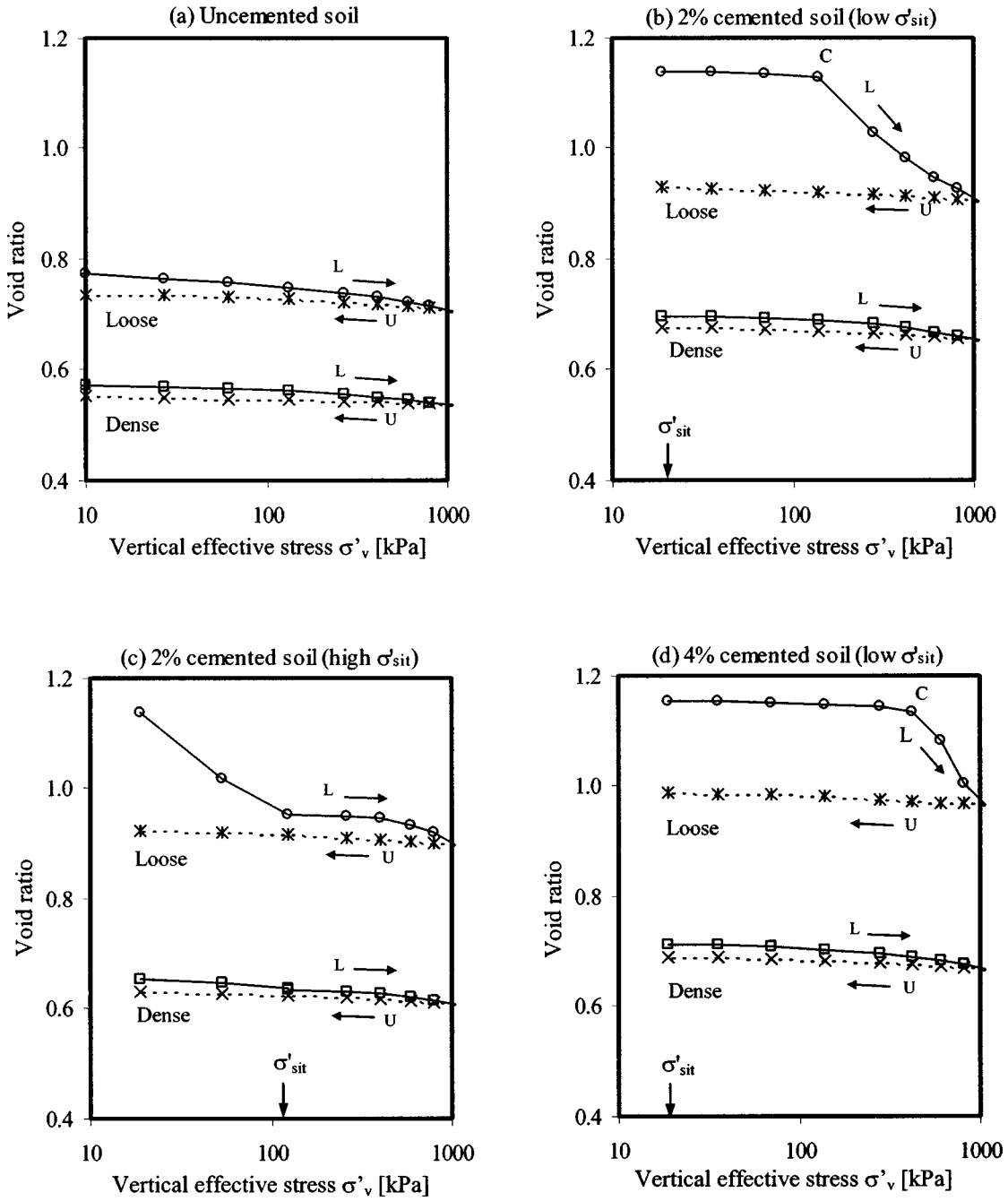

Fig. 6. Changes in void ratio with vertical effective stress in oedometric cell: (*L*) solid line loading, (*U*) dotted line unloading, and (*C*) collapse, (vertical sitting pressures during hardening σ'_{sit}=18.7 kPa, σ'_{sit}=122.8 kPa)

results confirm that the higher the cement content, the higher the specific surface of the sand–cement mixture, and the higher the suction for the same water content.

The velocity–stress sensitivity is lower in cemented specimens in the low-confinement regime than in uncemented soils. Velocity–stress trends appear to converge for both cemented and uncemented specimens at high confinement (see also Dvorkin et al. 1991).

Partial rather than massive decementation explains the higher stiffness of cemented specimens after collapse, as compared to uncemented specimens. Analytical results indicate that the shear wave velocity decreases as the size of cemented blocks decreases (Fratta and Santamarina 2002). In general, the higher the strain imposed during loading, the higher the stiffness loss that is observed upon unloading.

Fig. 8 summarizes observed trends in the log V_s versus log σ'_v space. Velocity–stress trends during unloading are not sketched in Fig. 8 for clarity. Results presented in Fig. 5 suggest that k_0 unloading renders higher velocity in uncemented soils, but lower velocities in cemented soils. This observation can be used as a diagnostic tool for sampling effects.

While load-induced collapse is considered herein, it is expected that similar methodology and observations can be applied to decementation collapse upon chemical changes, wetting, and dissolution (Abduljauwad and Al-Amoudi 1995).

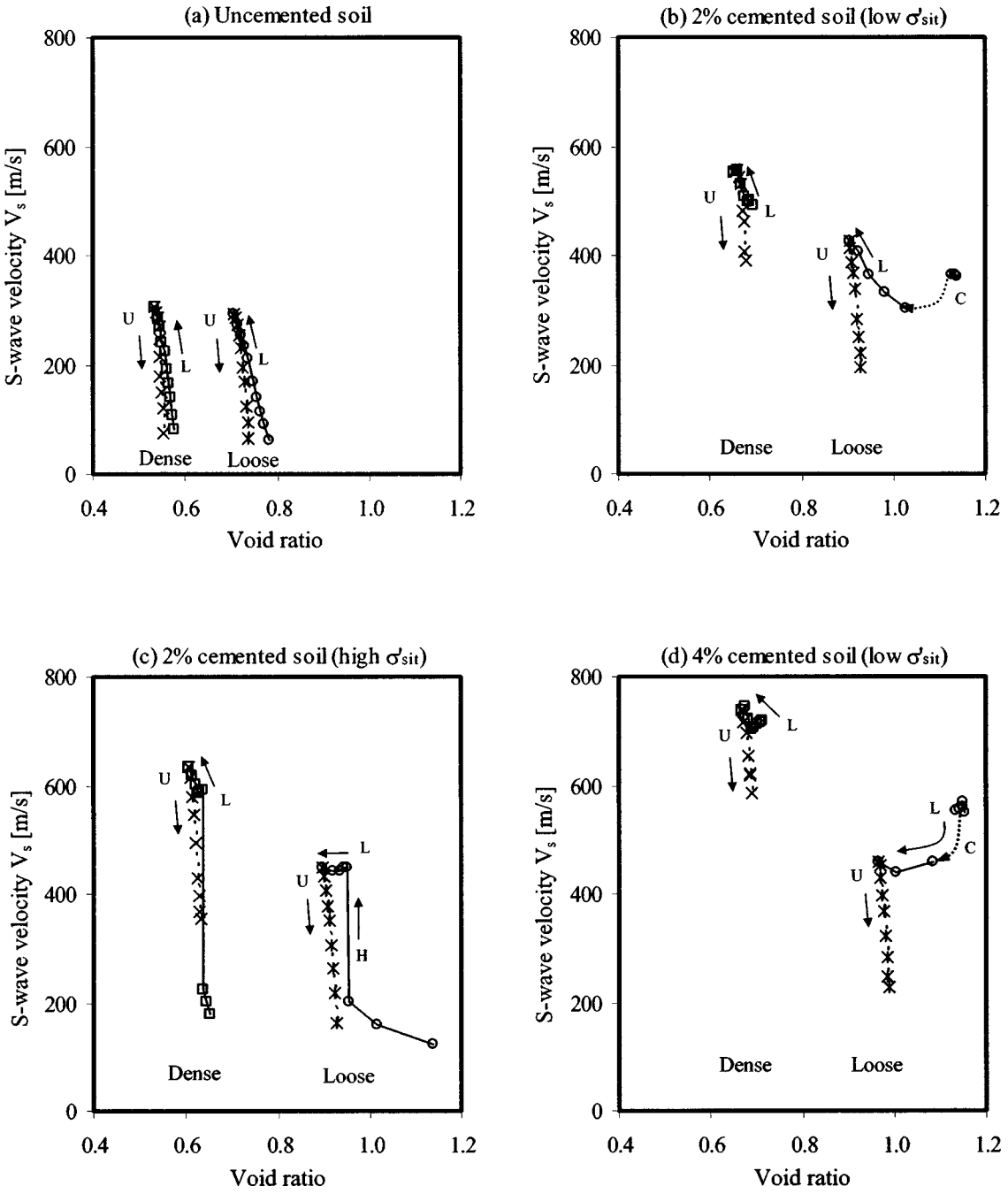

Fig. 7. Decementation softening and collapse: void ratio versus shear wave velocity: (*L*) solid line loading, (*U*) dotted line unloading, (*H*) hardening, and (*C*) collapse, (vertical sitting pressures during hardening $\sigma'_{sit}=18.7$ kPa and $\sigma'_{sit}=122.8$ kPa)

Conclusions

Published results show that the behavior of cemented soils depends on the amount and type of cement, the grain size distribution, the packing density of the soil, and the cementation–stress history. Cementation affects small-strain stiffness, dilative tendency during shear, liquefaction resistance, and both drained and undrained strengths. At high stress, all soil parameters gradually revert to the stress-controlled behavior that characterizes uncemented soils.

The small-strain stiffness is determined by the size of contact areas, i.e., flatness. Hence, even light cementation can have a more pronounced effect than confinement on the small-strain stiffness of hard-grained soils. Then, shear wave velocity provides valuable information about the degree of cementation, and the evolution of cementation and decementation in soils, without perturbing ongoing processes.

There is increasing interest in the design of shallow and deep foundations using small strain stiffness inferred from in situ shear wave velocity measurements. Such design approaches have resulted in much better agreement between predicted and measured settlements. However, results presented in this study show that loose, cemented materials may exhibit high initial stiffness but collapse upon loading, leading to large deformations.

Furthermore, loose, lightly cemented soils that experience load-induced collapse under k_0 conditions can exhibit small-strain

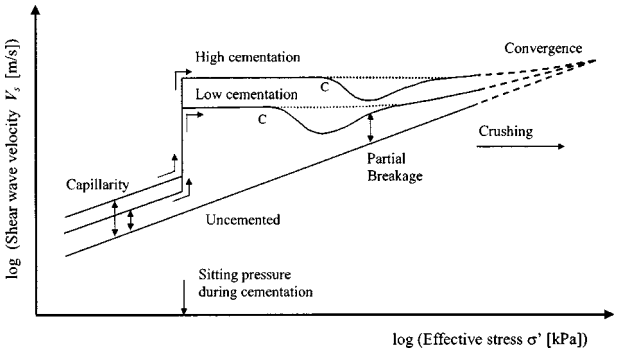

Fig. 8. Schematic trends—summary. Before cement hydration: fresh mixtures exhibit shear wave velocity higher than saturated uncemented soils due to capillarity. After cementation: low-cementation loose soil collapses at lower stress than high-cementation loose soil (solid lines correspond to loose specimens; "*C*" denotes collapse); dense cemented soil specimens do not collapse (dotted lines correspond to dense specimens). Very high confinement: shear wave velocity of cemented soils appears to asymptotically approach shear wave velocity of uncemented soils (dashed lines).

stiffness loss as a precursor to collapse. This observation may be used in the context of geophysics-based field monitoring (e.g., cross hole shear wave measurements normal to an ongoing excavation) within the framework of the observational method.

The higher the density, the cement content, and the effective confinement during cementation, the lower the possibility of decementation collapse during subsequent loading. Nevertheless, some breakage of interparticle bonds may take place even in the absence of collapse and a reduction of the small-strain stiffness is detected when the soil is k_0 unloaded to the same initial confinement.

The cemented soil behaves elastically, albeit not necessarily, linearly, during the early stages of loading. Stiffness, collapse load, and the corresponding threshold strain increase with cement content. While the small-strain stiffness determines the deformation before the collapse load, it is inadequate for predicting collapse deformation.

Acknowledgments

Support for this research was provided by the NSF Mid America Earthquake Center and The Goizueta Foundation.

References

Abduljauwad, S. N., and Al-Amoudi, O. S. B. (1995). "Geotechnical behavior of saline Sabkha soils." *Geotechnique*, 45(3), 425–445.

Acar, Y. B., and El-Tahir, A. (1986). "Low strain dynamic properties of artificially cemented sand." *J. Geotech. Eng.*, 112(11), 1001–1015.

Airey, D. W., and Fahey, M. (1991). "Cyclic response of calcareous soil from the north-west shelf of Australia." *Geotechnique*, 41(1), 101–121.

Baig, S., Picornell, M., and Nazarian, S. (1997). "Low strain shear modulus of cemented sands." *J. Geotech. Geoenviron. Eng.*, 123(6), 540–545.

Bernabe, Y., Fryer, D. T., and Hayes, J. A. (1992). "The effect of cement on the strength of granular rocks." *Geophys. Res. Lett.*, 19(14), 1511–1514.

Clough, G. W., Rad, N. S., Bachus, R. C., and Sitar, N. (1981). "Cemented sands under static loading." *J. Geotech. Eng. Div., Am. Soc. Civ. Eng.*, 107(6), 799–817.

Dass, R. N., Yen, S. S., Das, B. M., Puri, V. K., and Wright, M. A. (1994). "Tensile stress–strain characteristics of lightly cemented sand." *Geotech. Test. J.*, 17(3), 305–314.

Dupas, J. M., and Pecker, A. (1979). "Static and dynamic properties of sand-cement." *J. Geotech. Eng. Div., Am. Soc. Civ. Eng.*, 105(3), 419–436.

Dvorkin, J., Mavko, G., and Nur, A. (1991). "The effect of cementation on the elastic properties of granular material." *Mech. Mater.*, 12(3–4), 207–217.

Dvorkin, J., and Yin, H. (1995). "Contact laws for cemented grains: Implications for grain and cement failure." *Int. J. Solids Struct.*, 32(17), 2497–2510.

Dyvik, R., and Madshus, C. (1985). "Lab measurements of G_{max} using bender elements." *Proc., Advances in the Art of Testing Soils under Cyclic Conditions*, ASCE, New York, 186–196.

Fam, M., and Santamarina, J. C. (1995). "Study of geoprocesses with complementary wave measurements in an oedometer." *Geotech. Test. J.*, 18(3), 307–314.

Feda, J. (1982). *Mechanics of particulate materials*, Elsevier, New York.

Feda, J. (1994). "Collapse of soil structure." *Proc., Int. Symp. Engineering Characteristics of Arid Soils*, P. G. Fookes and R. H. G. Parry, eds., London, U.K., Balkema, Rotterdam, The Netherlands, 237–240.

Feda, J. (1995). "Behavior of cemented clay." *Can. Geotech. J.*, 32(5), 899–904.

Fernandez, A., and Santamarina, J. C. (2001). "Effect of cementation on the small strain parameters of sands." *Can. Geotech. J.*, 38(1), 191–199.

Fratta, D., and Santamarina, J. C. (2002). "Shear wave propagation in jointed rock—State of stress." *Geotechnique*, 52(7), 495–505.

Hardin, B. O., and Richart, F. E. (1963). "Elastic wave velocities in granular soils." *J. Soil Mech. Found. Div.*, 89(1), 33–65.

Jarrad, R. D., Niessen, F., Brink, J. D., and Bucker, C. (2000). "Effects of cementation on velocities of siliciclastic sediments." *Geophys. Res. Lett.*, 27(5), 593–596.

Kuwano, R., and Jardine, R. J. (2002). "On the applicability of cross-anisotropic elasticity to granular materials at very small strains." *Geotechnique*, 52(10), 727–749.

Lade, P. V., and Overton, D. D. (1989). "Cementation effects in frictional materials." *J. Geotech. Eng.*, 115(10), 1373–1387.

Landis, E. N., and Shah, S. P. (1995). "The influence of microcracking on the mechanical behavior of cement based materials." *Adv. Cem. Based Mater.*, 2, 105–118.

Leroueil, S., and Hight, D. W. (2003). "Behaviour and properties of natural soils and soft rocks." *Characterization and engineering properties of natural soils*, T. S. Tan, K. K. Phoon, D. W. Hight, and S. Leroueil, eds., Vol. 1, Balkema, Exton, Pa., 29–254.

Rao, S. M., Sridharan, A., and Ramanath, K. P. (1995). "Collapse behavior of an artificially cemented clayey silt." *Geotech. Test. J.*, 18(3), 334–341.

Reddy, K. R., and Saxena, S. K. (1993). "Effects of cementation on stress–strain and strength characteristics of sands." *Soils Found.*, 33(4), 121–134.

Richart, F. E., Hall, J. R., and Woods, R. D. (1970). *Vibrations of soils and foundations*, Prentice Hall, Englewood Cliffs, N.J.

Sánchez-Salinero, I., Roesset, J. M., and Stokoe, K. H. (1986). "Analytical studies of body wave propagation and attenuation." *Geotechnical Engineering Rep. No. GR86-15*, Univ. of Texas at Austin, Austin, Tex.

Santamarina, J. C., Klein, K. A., and Fam, M. (2001). *Soils and waves—Particulate materials behavior, characterization and process monitoring*, Wiley, Chichester, England.

Saxena, S. K., and Lastrico, R. M. (1978). "Static properties of lightly cemented sands." *J. Geotech. Eng. Div., Am. Soc. Civ. Eng.*, 104(12), 1449–1464.

Saxena, S. K., Reddy, K. R., and Avramidis, A. S. (1988). "Static behav-

ior of artificially cemented sand." *Indian Geotechnical J.*, 18(2), 111–141.
Schanz, T. (1998). "A constitutive model for cemented sands." *Localization and bifurcation theory for soils and rocks*, Balkema, Rotterdam, The Netherlands, 165–172.
Shibuya, S., Mitachi, T., Temma, M., and Kawaguchi, T. (2001). "Interrelationship between the metastability index and the undrained shear strength of six clays." *Advanced laboratory stress–strain testing of geomaterials*, F. Tatsuoka, S. Shibuya, and R. Kuwano, eds., Swets & Zeitlinger, Lisse, The Netherlands, 111–186.
Shirley, D. J., and Hampton, L. D. (1978). "Shear wave measurements in laboratory sediments." *J. Acoust. Soc. Am.*, 63(2), 607–613.
Sienkiewicz, F., Shukla, A., Sadd, M., Zhang, Z., and Dvorkin, J. (1996). "A combined experimental and numerical scheme for the determination of contact loads between cemented particles." *Mech. Mater.*, 22, 43–50.
Tatsuoka, F., and Shibuya, S. (1991). "Deformation characteristics of soils and rocks from field and laboratory tests." *Proc., 9th Asian Regional Conf. Soil Mechanics and Foundation Engineering*, Bangkok, Vol. 2, 101–177.
Thomann, T. G., and Hryciw, R. D. (1990). "Laboratory measurement of small strain shear modulus under k_0 conditions." *Geotech. Test. J.*, 13(2), 97–105.
Winkler, K. W. (1983). "Contact stiffness in granular porous materials: Comparison between theory and experiment." *Geophys. Res. Lett.*, 10(11), 1073–1076.
Wissa, A. E. Z., and Ladd, C. C. (1965). "Shear strength generation in stabilized soils." *Rep. No. R65-17, Soils Publication No. 173*, M.I.T., Cambridge, Mass.
Yin, H., and Dvorkin, J. (1994). "Strength of cemented grains." *Geophys. Res. Lett.*, 21(10), 903–906.
Zang, A., and Wong, T.-F. (1995). "Elastic stiffness and stress concentration in cemented granular material." *Int. J. Rock Mech. Min. Sci. Geomech. Abstr.*, 32(6), 563–574.